



Novel nanocomposites based on chlorinated styrene butadiene rubber and manganous tungstate: focus on curing, mechanical, electrical and solvent transport properties

V. C. Jasna¹ , T. Anilkumar¹ , G. Mathew² , and M. T. Ramesan^{1,*}

¹Department of Chemistry, University of Calicut, Calicut University P.O., Thenhipalam, Kerala 673635, India

²Department of Chemistry, St. Marys College Wayanad, S. Bathery, Kerala 673592, India

Received: 8 January 2018

Accepted: 26 March 2018

Published online:

2 April 2018

© Springer Science+Business Media, LLC, part of Springer Nature 2018

ABSTRACT

The present work investigates the influence of loading of manganous tungstate (MnWO_4) nanoparticles on the rheometric processing characteristics, crystallinity, morphology, glass transition temperature, oil resistance, transport behavior, mechanical and electrical properties of chlorinated styrene butadiene rubber (Cl-SBR). The reduction in the overall amorphous nature of Cl-SBR has been observed with the addition of nanofillers, as confirmed by X-ray diffraction studies. The maximum uniform dispersion of nanofiller in Cl-SBR has been noted at 7-phr loading, while at higher loadings, filler agglomerations have been observed in the scanning electron micrographs. An increase in the glass transition values with the addition of nanoparticles proves the reduced flexibility of the elastomer systems. The reduction in optimum cure time with the loading of nanoparticles has been found to be beneficial as far as the production rate of articles using these nanocomposites is concerned. Among the mechanical properties studies, tensile strength, modulus and tear strength registered an increase in the loading of nanofillers up to 7 phr due to the reinforcement of elastomer by the nanoparticles. The AC conductivity of Cl-SBR/ MnWO_4 nanocomposite increased with increasing the frequency and loading of nanoparticles. It is important that at 7-phr loading of nanoparticles, the conductivity value reaches the range of semiconductors. The superior reinforcement of Cl-SBR with 7-phr nanoparticles has been supported by the results of solvent diffusion and transport studies also. Values of solvent sorption parameters such as the energy of activation and enthalpy of diffusion have been found to be complementary to each other supporting the results obtained earlier. The reinforcing ability of the nanoparticles in Cl-SBR has been correlated with Lorentz and Park model.

Address correspondence to E-mail: mtramesan@hotmail.com

Introduction

Academic and industrial research works have paid great energy and money to the fascinating field of polymer nanocomposites. The main reason for this is obviously the superior performance to weight ratio, which is unique for these materials [1–3]. Polymers reinforced with nanomaterial exhibited mechanical strength, modulus, high thermal stability, improved barrier properties and flame resistance [4–6]. They offer superior performance and durability compared to conventional composites. This wide range of properties is determined by various factors of the reinforcing filler, such as size, shape, surface morphology and the effectiveness filler particles distribution in the polymer matrix [7–9]. In other words, the polymer–nanofiller interface plays the major role in deciding these useful properties. The large interfacial area per unit volume and low weight will impart the distinguished reinforcement of nanocomposites [10]. In the literature, much attention has been focused on the electrical properties, namely the conductivity and the dielectric properties [11–13]. Owing to the requirement of the market for novel semiconducting material with easy processability, polymeric insulating material filled with electrically conducting metal nanoparticles has gained much attraction in recent years [14]. Researchers, in specific cases [15], revealed that the electrical conductivity of the polymer nanocomposites depends on nature of filler and polymer, loading of filler, dispersion of filler and crystallinity of nanoparticles. In this scenario, the use of elastomers, which are of low modulus, easily processable, curable and compliant, is most promising. Several polymers have been used for preparing polymer nanocomposites such as natural rubber, epoxidized natural rubber, SBR and chloroprene rubber [16–19]. Among these, SBR is unique due to its purely synthetic nature and resulting well-defined properties and possibilities for further chemical modification due to the unsaturation of the butadiene repeating unit.

Styrene butadiene rubber (SBR) is widely employed in the tire industry, healthcare products and cables [20, 21]. Despite its high abrasion resistance, SBR suffers from poor tensile strength, flame retardancy and very low oil resistance. Research focusing on the reinforcement of SBR with nanoparticles also did not give fruitful results due to the poor

mechanical properties resulting from the weak interface formed between the elastomer and nanoparticles. One of the many strategies to enhance the interfacial interaction between SBR and nanofiller is by the incorporation of the polar functional group in the rubber. Our previous research showed that chemically modified SBR (chlorinated SBR) has excellent tensile strength, tear property and flame-retardant behavior. Chlorination improved its oil resistance superior to that of chloroprene rubber and equal to that of nitrile rubber [22, 23].

Polymer nanocomposites can be prepared by many methods such as solution mixing, melt mixing or by using simple and efficient two-roll open mill mixer. Solution mixing gives a uniform dispersion of nanofiller in the elastomer matrix, but the occlusion of solvent in the matrix reduces the glass transition temperature of the nanocomposite, plasticizes the sample and deteriorates its properties, so as to affect health, thereby limiting industrial applications. The problem with melt mixing is the possible rupture of the polymer chain and the resulting reduction in molecular weight and degradation in the random mode. Compared to these methods, simple two-roll mill mixing method is relatively quick and easy and results in a superior performance of the final product [24, 25].

In this study, we report the novel elastomer nanocomposites based on chlorinated SBR and MnWO_4 . A simple open two-roll mixing mill is used for the preparation of the sample. The main objectives of the present investigation are to analyze the effect of MnWO_4 nanoparticles on the curing properties, structural, morphological, thermal, mechanical and electrical properties of the resulting nanocomposite. This study is also focused on the effect of manganous tungstate nanofiller on the absorption of ASTM oils and on the transport of petroleum fuels through vulcanized chlorinated SBR at different temperatures, thus calculating the overall performance of the nanocomposites. Also, the extent of reinforcement has been correlated with a theoretical model.

Experimental

Materials and methods

Chloroform, manganous chloride, sodium tungstate, sodium hydroxide, isopropyl alcohol and cetyltrimethylammonium bromide (CTAB) were

purchased from Merck, India. The solvents like petrol (mol wt 100), kerosene (mol wt 170) and diesel (mol wt 230) were of reagent grade procured from Bharat Petroleum Corporation Limited, India. SBR (Synaprene 1502) was procured from Synthetics and Chemicals Ltd., India. Rubber ingredients such as zinc oxide (ZnO), stearic acid, 2, 2, 4-trimethyl-1,2-dihydroquinoline (TDQ), *N*-cyclohexyl-2-benzothiazole sulfenamide (CBS), tetramethylthiuram disulfide (TMTD), processing oil and sulfur were used for the fabrication of Cl-SBR/MnWO₄ composites. Oil resistance of the vulcanized samples was tested by ASTM oils No. 1, 2 and 3.

Preparation of chlorinated SBR

Chlorinated SBR with 15% chlorine content was prepared from SBR by the situ reaction of chloroform with aqueous caustic soda using phase transfer catalysis (CTAB), as reported earlier [23]. Briefly, SBR was dissolved in toluene, the phase transfer catalyst (CTAB) was added to this, and the solution was stirred well. To this, CHCl₃ was added dropwise followed by an aqueous NaOH solution. The chlorinated SBR was separated from the solution by coagulating it with isopropyl alcohol and dried.

Preparation of MnWO₄ nanoparticles

MnWO₄ nanoparticles were prepared by the chemical co-precipitation technique [26]. Equimolar ratios of manganous chloride and sodium tungstate were dissolved in distilled water separately. Then, cetyltrimethylammonium bromide in aqueous solution was added to the manganous chloride solution with constant stirring. Sodium tungstate solution was added dropwise to the above mixture with continuous stirring. The precipitated product was washed with water several times and dried. The dried powder was then calcined at 800 °C for 5 h.

Preparation of Cl-SBR/MnWO₄ nanocomposites

Chlorinated SBR/MnWO₄ nanocomposites were prepared at room temperature by a mill mixing technique. Compounding of Cl-SBR with different loadings of MnWO₄ nanoparticles [0, 3, 5, 7, 10 and 15 parts per hundred parts rubber (phr)] was carried out in an open two-roll mixing mill. The rotors operated

at a friction ratio of 1:1.4. Rubber nanocomposites were prepared by mixing rubber with 5.0 phr of ZnO, 2.0 phr of stearic acid, 1.0 phr of TDQ, 1.2 phr of CBS, 0.8 phr of TMTD and finally 2.2 phr of sulfur. The vulcanization ingredients were added to the rubber before the addition of the nanoparticles, and finally, the sulfur was added. The compounding was carried out at room temperature in accordance with the ASTM D-15-627 (1994) method, with a special attention to maintain the uniform distribution of nanoparticles. Here we use the sample code as CSM₀ is Cl-SBR with no filler loading CSM₃, CSM₅, CSM₇, CSM₁₀ and CSM₁₅ are polymer composite with 3, 5, 10 and 15 phr of MnWO₄ nanoparticles.

Characterizations

X-ray diffraction studies of the nanocomposite samples were carried out using Rigaku MiniFlex 600 diffractometer. The XRD was recorded in terms of 2θ in the range 10°–80°. The surface morphology of the fabricated polymer nanocomposites was analyzed by a Hitachi S-3000 H scanning electron microscope. Differential scanning calorimetry (DSC) was done by Mettler-Toledo DSC 22e at a heating rate of 10 °C/min (atmosphere N₂; flow 40 ml/min). The alternating current (AC) and dielectric loss of the gum and elastomeric nanocomposites were determined by a fully automatic Hewlett-Packard LCR meter (HP: 4284A) from the frequency range of 10²–10⁶ Hz. Vulcanization properties were studied by a Monsanto Rheometer R-100 at 150 °C according to ASTM D 2705. The rubbery materials were molded to their respective optimum cure times in an electrically heated (150 °C) hydraulic press at a pressure of 40 MPa. From the vulcanized sheets, dumb-bell-shaped and angle-shaped specimens were punched out and the tensile strength and tear resistance of the elastomer composite vulcanizates were carried out at a crosshead speed of 500 mm/min using a Zwick Universal Testing Machine (UTM) at room temperature as per the ASTM D 412-80 and ASTM D 624-81, respectively. In this work, an average of five samples was used to study the tensile and tear properties. The hardness of the nanocomposite vulcanizate was measured according to ASTM D 2240-95 using a Shore A-type durometer. Using a Dunlop tripsometer, the rebound resilience was measured as per the ASTM D 1054. Heat buildup of the vulcanized samples was determined by Goodrich flexometer

according to ASTM D 623. The abrasion resistance of the samples was carried out in a DIN abrader according to DIN 5351 standard. For oil resistance studies, the vulcanized samples of MnWO₄/chlorinated SBR composites were immersed in ASTM # 1, 2 and 3 oils at room temperature (25 °C). After 72 h of oil immersion, the samples were taken out, dipped in acetone and wiped off with filter paper to remove excess oil from the surface. The oil uptake was assessed gravimetrically. The solvent imbibing and transport mechanism of Cl-SBR/MnWO₄ nanocomposites were carried out by cutting the circular-shaped samples from the vulcanized sheets. The thickness of the samples was measured using a screw gauge, and the weighed samples were immersed in different hydrocarbon solvents like petrol, diesel and kerosene taken in the diffusion bottles. Weigh the samples in particular time intervals and again put in the solvents. The weighing of the sample was continued up to equilibrium weight obtained. These studies were carried out at different temperatures at which nanocomposite samples are expected to serve in service life. The diffusion experiments were conducted duplicates or triplicates in most cases, and the standard deviation was within ± 0.08 – 0.1 mole percentage (mol%).

Results and discussion

X-ray diffraction analysis (XRD)

X-ray diffraction patterns of MnWO₄, Cl-SBR and Cl-SBR/MnWO₄ nanocomposites are displayed in Fig. 1. Many crystalline peaks of MnWO₄ are observed from the XRD which corresponds to monoclinic wolframite tungstate structure, and this is consistent with values taken from the literature [27] (JCPDS Card Number: 80-0133). The average crystallite size of MnWO₄ powder has been estimated automatically from corresponding XRD data using Scherrer formula, $D = 0.94\lambda / \beta \cos\theta$, and the average crystallite size is 28 nm. The XRD pattern of Cl-SBR shows the broad peak centered at $2\theta = 21.2^\circ$ indicating the amorphous nature of the polymer and a weak XRD peak at $2\theta = 29.36^\circ$ associated with the crystalline unit of the Cl-SBR. The prepared Cl-SBR/MnWO₄ composite contains most of the diffraction peaks of MnWO₄ and Cl-SBR. It is clear from the figures that the amorphous nature of Cl-SBR has

decreased with the addition of MnWO₄ nanoparticles. In addition to this, it can be seen from a comparison of nanocomposite with the Cl-SBR that the diffraction peak of MnWO₄ in the polymer matrix is slightly shifted from lower diffraction angle to higher one. This indicates the structural changes of composites by the interaction of elastomer with the nanoparticles, and these results are in good agreement with the previous studies [28, 29].

Scanning electron microscopy (SEM)

The degree of MnWO₄ nanoparticles dispersion in Cl-SBR with its varying loadings is examined by SEM, and images are given in Fig. 2. From Fig. 2a, it can be seen that the SEM image of Cl-SBR presents a weak matrix with some irregular shape and domain size of the elastomer. This irregular morphology of Cl-SBR is totally changing with the addition of 7-phr MnWO₄ nanofiller (Fig. 2b). It can be deduced that insertion of MnWO₄ imparts uniform dispersion of nanoparticles in the polymer matrix. The uniform nature of the composite is due to the strong intermolecular interaction between MnWO₄ nanoparticles and the Cl-SBR chain. As shown in Fig. 2c, at higher loading of MnWO₄ (15 phr), the uniform morphology of nanocomposite changes its characteristics to a highly branched and interlinked morphology with slight agglomeration of nanoparticles.

Differential scanning calorimetry (DSC)

Glass transition temperature (T_g) obtained from DSC analysis is important in deciding the range of service temperature of polymeric materials and is used for evaluating the flexibility of a polymer molecule. The DSC thermograms of Cl-SBR and Cl-SBR with different contents of MnWO₄ nanoparticles are given in Fig. 3. All the samples show two glass transition temperatures. The first thermal transition observed at -53°C is attributing to the glass transition temperature of SBR, and second T_g appearing at -35.1°C is assigned to the chlorinated segment of SBR [22]. Chlorinated moieties in SBR have lower flexibility, and this causes an increase in T_g of SBR from -53 to -35.1°C . It is well recognized that the T_g of polymer composite depends on the overall flexibility of the chains resulting from the interfacial interactions between the nanofiller and the polymer, crystallinity and polarity of filler particles. It is clear from the

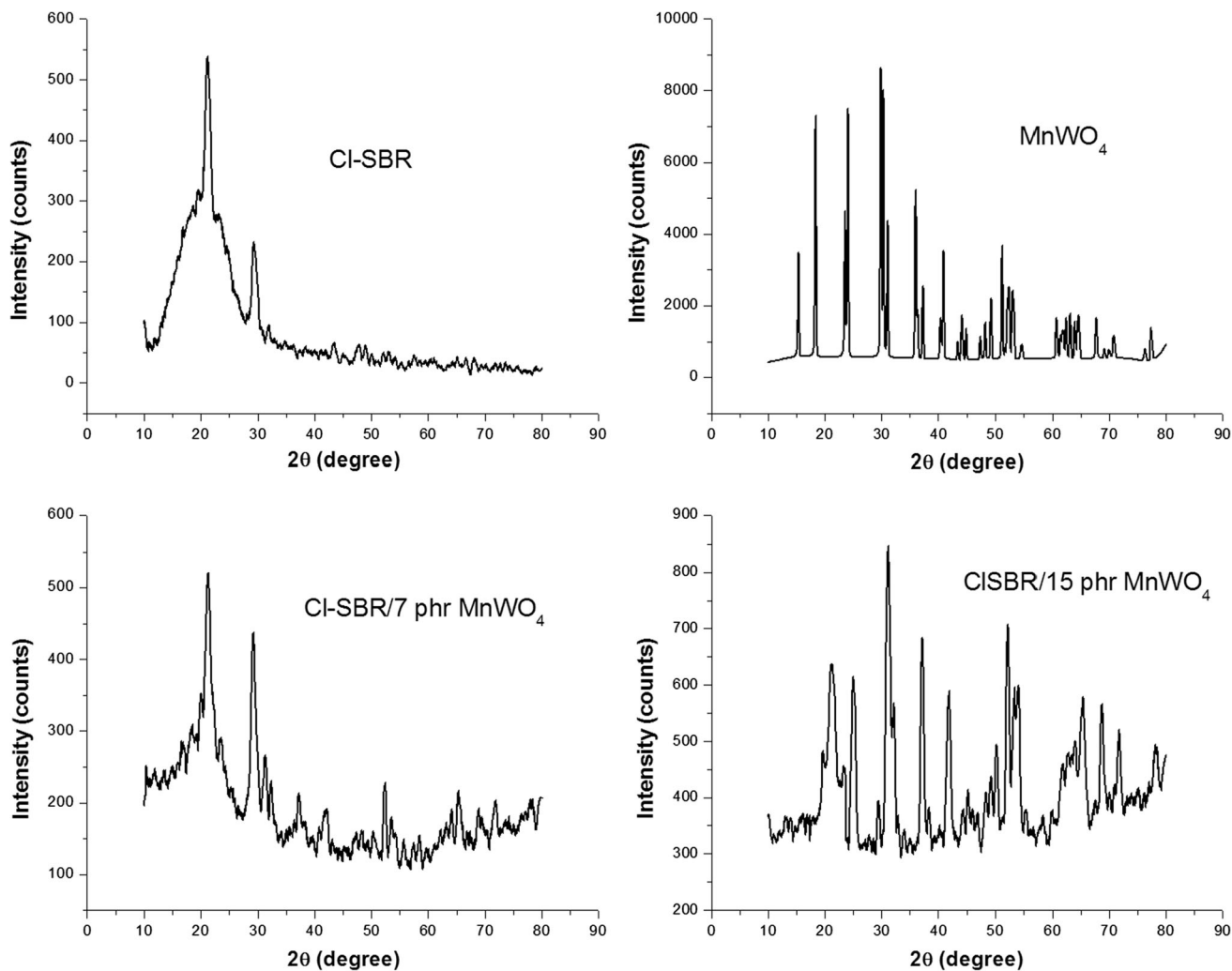


Figure 1 XRD pattern of MnWO_4 , CI-SBR and different contents of MnWO_4 /CI-SBR.

figure that the glass transition temperatures of all nanocomposites are higher than that of pure CI-SBR. This confirms the reduced flexibility of CI-SBR chains resulting from its reinforcement by MnWO_4 nanoparticles. The composites with 5, 10 and 15 phr samples showed the T_g at -33.9 , -32.8 and -29.39 °C, respectively. The rise in T_g of nanocomposites is due to the strong intermolecular interactions between the nanoparticles and the polymer chains. At higher loading, the segmental movement of polymer chains is restricted, which causes an enhancement in the T_g of polymer composites [30]. It is important to mention here that the loading of nanoparticles does not affect the glass transition temperature of SBR units at -53 °C. This suggests that the efficient interfacial interaction is taking place between the chlorinated polar units of SBR with MnWO_4 .

Cure characteristics

The cure characteristics of the different CI-SBR/ MnWO_4 nanocomposites are shown in Table 1. The minimum torque value M_L is considered as the measure of viscosity resulting from the filler content in the polymer matrix. It is always expected to increase with the loading of nanoparticles, and the same observation can be seen here [26]. The maximum torque value (M_H) is the measure of the combined effect of physical reinforcement of filler in polymer and the cross-link density of the vulcanizate [31]. It can be seen that both maximum and minimum torque values of the uncured CI-SBR/ MnWO_4 composites increase with the loading of nanoparticle up to 7 phr. This indicates the maximum polymer filler adhesion at 7-phr loading of nanofiller, due to strong intermolecular interactions. The decrease in

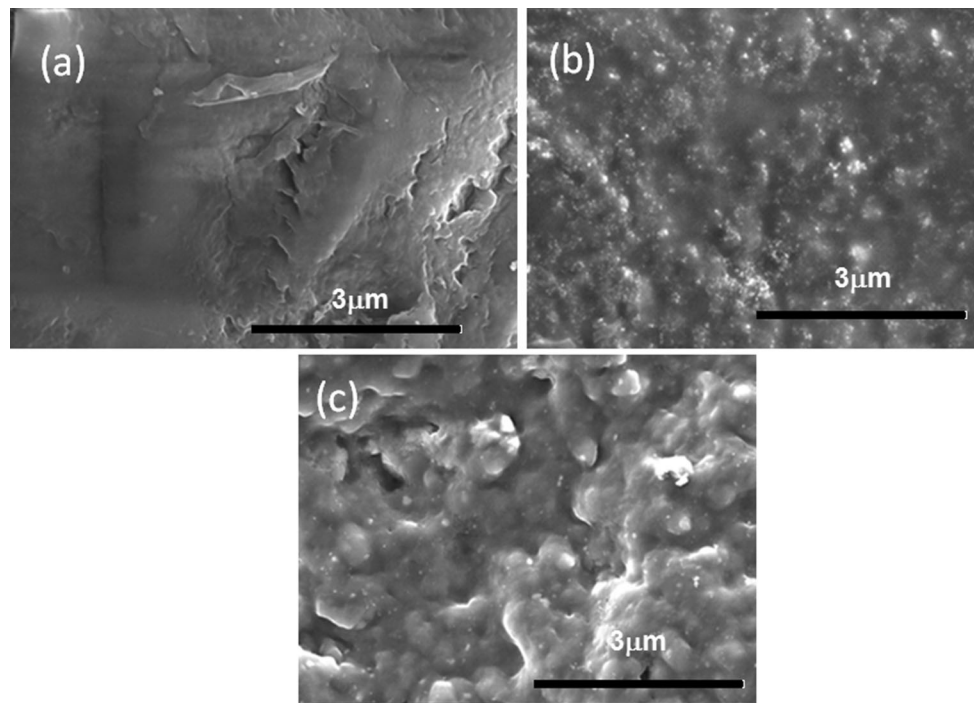


Figure 2 SEM images of **a** CI-SBR, **b** CI-SBR with 7 phr and **c** 15-phr MnWO_4 nanoparticles.

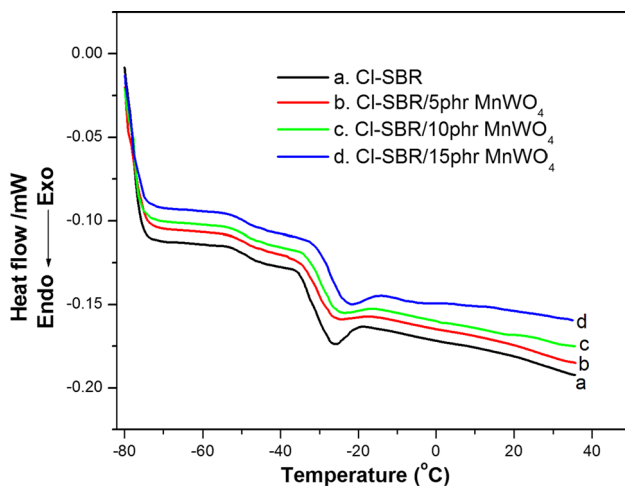


Figure 3 DSC thermograms of CI-SBR and CI-SBR with different contents of MnWO_4 .

rheometric torques with further loading is attributed to the diluent effect and agglomeration of nanoparticles resulting in poor cross-links between the CI-SBR and MnWO_4 nanoparticles. Scorch time is the time required for the torque value to increase by 5 units above the minimum torque value, and it is a direct measure of the scorch (premature vulcanization time) safety of the nanocomposite samples. The optimum cure time t_{90} is the time for the

vulcanization form 90% of the cross-links to get better physical properties. It can be seen from the table that both scorch and optimum cure time decrease regularly with an increase in the concentration of MnWO_4 nanoparticles. This is because of the dual role of metal nanoparticles primarily as co-activators and secondarily facilitating the heat transfer in the system creating more interaction with the curing agent. These factors ultimately lead to better cross-linking in the CI-SBR matrix. The reduction in optimum cure time is advantageous because it can enhance the production rate of articles made from these elastomer nanocomposites.

Mechanical properties

The incorporation of nanoparticles into a weak elastomer matrix such as SBR is a highly effective technique to improve its mechanical properties. The tensile strength, modulus, elongation at break, tear resistance, hardness, abrasion loss, resilience and heat buildup of CI-SBR with different loadings of MnWO_4 nanoparticles are given in Table 2. The tensile properties of polymer/nanofiller vulcanizates depend on several factors such as the uniform dispersion of nanoparticles, the compatibility between filler and polymer, polarity and crystalline nature of

Table 1 Processing characteristics of Cl-SBR and Cl-SBR with different loadings of MnWO₄ nanofiller

Sample code	Cure time, t_{90} (min)	Scorch time, t_2 (min)	Maximum torque, M_H (dNm)	Minimum torque, M_L (dNm)
CSM ₀	14	4.0	34	9.25
CSM ₃	12.7	3.82	36.5	10.2
CSM ₅	11.8	3.60	40.4	11.3
CSM ₇	11.0	3.48	45.0	12.2
CSM ₁₀	10.0	3.29	43.6	11.6
CSM ₁₅	9.2	3.05	42.8	10.3

fillers [32]. For Cl-SBR/MnWO₄ nanocomposites, tensile strength, modulus at 300% and tear resistance increased with the increase in the concentration of MnWO₄ reaching the maximum value up to 7-phr loading. Further addition of nanofillers reduces these values. The higher tensile, tear and modulus values at 7-phr loading of MnWO₄ are due to the uniform dispersion of the nanofiller and the strong interaction of nanoparticles with the elastomeric chains. The optimization of interaction between the chlorinated moieties in Cl-SBR and MnWO₄ filler particles brings excellent compatibility between the chain segments and nanoparticles. The decrease in tensile and tear properties beyond 7-phr loading is due to the combined influence of the clustering tendency and a possible dilution effect. These results are in good agreement with several reported works [33–35]. The force applied to pull the vulcanizate apart is measured to determine the elongation at break (EB), and the values of EB are given in Table 2. The EB decreases with the addition of nanoparticles in all the systems, and it is well recognized that the decreased EB is an indication of the higher reinforcement of nanoparticles in the polymer matrix [36]. Shore hardness becomes an important property when the

surface property of nanocomposite becomes relevant. The hardness of the Cl-SBR/MnWO₄ nanocomposite is also given in Table 2. It shows a progressive increase in hardness of compound with the loading of nanoparticles. This is usual to expect from the addition of a high modulus material to a low modulus material such as Cl-SBR. Abrasion resistance is the material property to prevent the rubbing or scraping that tends to remove material from its surface, and the abrasion resistance value of elastomeric composite is given in Table 2. Nanoparticles incorporated polymer has lower abrasion loss than the pure Cl-SBR. Rebound resilience is the compound ability to retain its original dimensions and shape after temporary deformation. Resilience values of Cl-SBR with different loading MnWO₄ filler are given in Table 2. The resilience decreases with the loading of nanoparticles as expected. Heat buildup is the increase in temperature of the specimen when it is subjected to an oscillating compressive stress cycle in a controlled environment. The heat buildup values of Cl-SBR and Cl-SBR/MnWO₄ nanocomposites are shown in Table 2. The heat buildup of composite increases with the increase in loading of

Table 2 Mechanical properties of Cl-SBR and Cl-SBR with various contents of MnWO₄ nanoparticles

Properties	Loading of MnWO ₄ nanoparticles (phr)					
	0	3	5	7	10	15
Tensile strength (MPa)	7.45	9.66	13.21	18.01	16.34	13.02
Elongation @ break (%)	398	366	348	335	319	292
Modulus (300%)	2.44	3.16	5.72	8.02	7.69	6.51
Tear strength (kN/m)	27.3	29.3	32.9	37.0	35.9	34.4
Hardness (Shore A)	35	36	37	38	41	43
Heat buildup (°C)	12.3	13.0	14.4	15.5	16.6	17.0
Compression set (%)	12.6	13.8	15.1	15.5	15.1	14.3
Abrasion loss (mm ³)	77.0	76.1	75.6	75.2	74.7	74.0
Resilience (%)	36.3	34.7	31.9	29.6	28.1	26.5

nanoparticles due to more extensive cross-linking achieved through better thermal conductivity.

Oil resistance

Fuel and oil-resistant elastomeric compounds and nanocomposites are promising materials for automotive industry. Without coming in contact with fuels, greases and oils, the life cycle of an automotive product will not be completed. The solvent and oil resistance properties are inherent rubbers containing polar functional groups. These include chloroprene, chlorinated SBR and NBR. The oil resistance (ASTM oil # 1, 2 and 3) shown by CI-SBR and its nanocomposites at various temperatures are given in Fig. 4. All the composite shows higher oil resistance values than the CI-SBR control sample. Among the nanocomposites, vulcanizate containing 7-phr MnWO_4 nanofiller shows the maximum oil resistance at 25 and at 100 °C. Various factors such as the electro-negativity of rubber compounds, cross-link density and crystallinity play an important role in deciding the oil resistance of samples [22]. The higher oil resistance of nanocomposite in the present study is due to the uniform dispersion of crystalline MnWO_4 particles. The clustering of nanoparticles in CI-SBR matrix beyond 7 phr decreases cross-link density of the polymer matrix. The oil resistance of all the samples decreases with increasing temperatures due to easy penetration of oil into the thermally relaxed polymeric matrix. It is clear from the

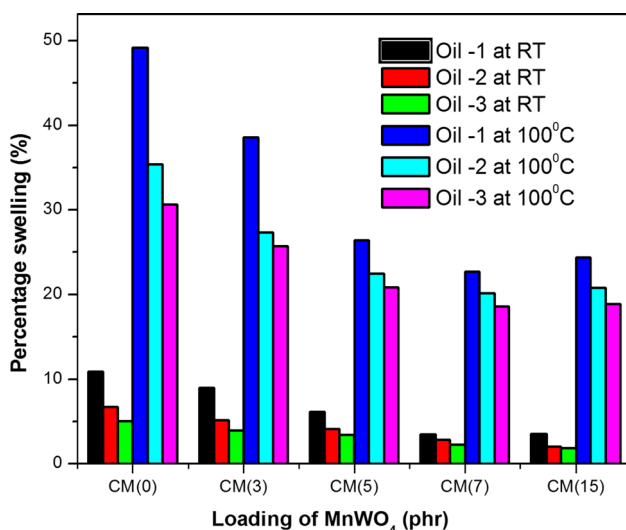


Figure 4 Oil resistance of CI-SBR with different contents of MnWO_4 .

figure that the penetration of oil is more pronounced in ASTM oil # 3 than oil # 1 and oil # 2. This is because the aniline point of ASTM oil # 3 is significantly lower, and therefore, it diffuses more easily into the nanocomposites.

AC conductivity studies

In certain uses such as electrical insulation of household items using polymer, polymer blend or composites, the polymer material needs to withstand only low-frequency AC. However, if the polymer needs to be used for insulating high frequency for example, as in radars, different polymers such as polyethylene must be employed. Therefore, the variation of AC conductivity as a function of frequency deserves much importance. Also during service, polymeric materials may have to perform under various frequencies. Figure 5 represents the frequency dependence of alternating current (AC) conductivity of CI-SBR and CI-SBR/ MnWO_4 nanocomposites with different filler loadings. The conductivity shows an increase in trend with an increasing frequency for all the samples. It is clear that the conductivity of nanocomposites is greater than that of pure CI-SBR. The randomly oriented macromolecular chains of CI-SBR (confirmed from XRD) provide a poor compactness of the polymer, leading to its low conductivity. The conduction mechanism of polymer composite normally occurs in two ways: (1) tunneling effect between the conductive fillers separated by the polymer layer and (2)

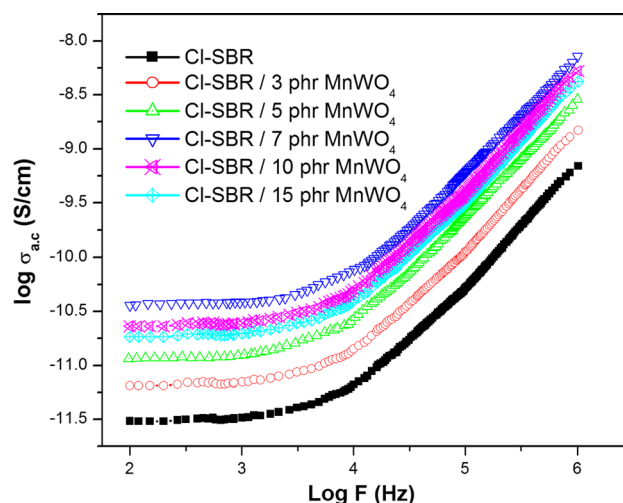


Figure 5 AC conductivity of CI-SBR and CI-SBR/ MnWO_4 nanoparticles.

through the flow of electrons through the conductive network. In the present study, the tunneling mechanism is the major factor affecting the conductivity of the elastomeric materials and these results are in accordance with the earlier study [37]. Moreover, uniform dispersion of nanoparticles in the polymer and the interfacial polarization between the nanoparticles and polymer chain are also affecting the electrical conductivity of polymer composites. Also, the conductivity increases with the loading of nanoparticles up to 7-phr loading. The higher conductivity of nanocomposite at 7-phr loading is due to the strong intermolecular interaction between the nanoparticles and the chlorinated segments of SBR. Due to these strong interactions, the crystalline MnWO₄ imparts a structural order in the composites, thereby leading to a higher conductivity. As the loading of nanoparticles increased above 7 phr, the AC conductivity of nanocomposite is found to be decreasing. At higher loading, the nanoparticles are oriented irregularly making the linkage between the polymer matrixes very poor which leads to poor conductivity. This is clear from the SEM photographs presented earlier.

Dielectric loss tangent (Tan δ)

The amount of dissipated energy or the electrical loss by an insulating material when a voltage is applied to the material can be represented by means of dielectric loss factor (Tan δ). Usually, this occurs due to two main reasons such as relaxation effect and resonance. The variation of dielectric loss as a function of frequency for CI-SBR and CI-SBR/MnWO₄ nanocomposites at room temperature is shown in Fig. 6. It has been observed that the values of Tan δ decrease in the low frequency region from 10² to 10⁴ Hz and remain constant for all the composites up to the applied frequency above 10⁴ Hz. Generally, more energy is required for the polarization of grain boundaries at a lower frequency and therefore the energy loss is higher for the composite materials [38]. However, the polarization between the grain boundaries is minimum at higher frequencies which lower the Tan δ values. It can be seen from the figure that the tangent loss increases with the loading of nanoparticles up to 7-phr loading due to the strong interaction between the polymer and the nanoparticles. Generally, the maximum tangent loss (Tan δ) occurred when the migration and accumulation of charge carriers are

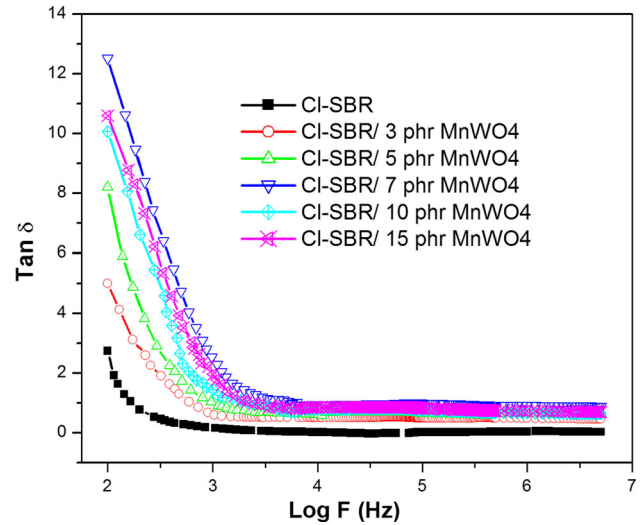


Figure 6 Dielectric loss tangent plots of CI-SBR and CI-SBR MnWO₄ nanocomposite.

maximum at the interface between nanofiller and the polymer matrix. Nanoparticles undergo agglomerations at higher loading (above 7 phr), which resist the migration and accumulation of charge carriers leading to a poor interfacial polarization. Therefore, the dielectric loss tangent decreases at higher loading of fillers.

Diffusion studies

The sorption results were expressed as mol percentage uptake of solvents by 100 grams of sample (Q_t mol%)

$$Q_t(\text{mol}\%) = \frac{\text{mass of solvent sorbed} / \text{molecular weight of penetrant}}{\text{initial weight of polymer sample}} \times 100 \tag{1}$$

The effect of filler contents on swelling properties of CI-SBR and CI-SBR/MnWO₄ in petrol at 27 °C is shown in Fig. 7. It can be seen that all the plots are sigmoidal in nature signifying the initial high uptake of the solvent followed by the slow uptake that slowly reaches the equilibrium. As the filler concentration increases, the solvent uptake decreases as expected from the reinforcement [39]. The composite with 7 phr of MnWO₄ possesses very low rate of uptake. The free volume inside the CI-SBR matrix decreases with the addition of nanoparticles; hence, the mobility of solvent inside the polymer chain is

restricted and this decreases the mol uptake [40]. At a higher loading of nanoparticles above (7 phr), the solvent uptake increases due to agglomeration of MnWO_4 . All the curves at room temperature, in petrol, diesel and kerosene show the same trends.

The effect of solvent on sorption mainly depends on the structure, molecular weight and polarity of solvent molecules. Figure 8 shows the effect of various solvents such as petrol, diesel and kerosene in the uptake of Cl-SBR/7 phr MnWO_4 . It is clear that the solvent uptake decreases with increasing the size of the penetrant molecules, i.e., from petrol to diesel solvent uptake decreases. This can be explained on the basis of free volume theory, according to which the diffusion [41] rate of penetrant molecules depends on the ability of polymer segments to exchange their voids to the penetrant molecules. Owing to the presence of reinforcing fillers, the exchange of positions in the macromolecular chain becomes very difficult for large penetrant molecules which agree with many previous studies [42–44].

The increase in temperature as expected can enhance the solvent uptake. Figure 9 shows the effect of temperature on mol uptake of petrol at 27, 40 and 50 °C, respectively. The composite having maximum solvent-resistant property (7 phr of filler) is selected to analyze the effect of temperature. An increase in solvent uptake with the increase in temperature can be observed; it is due to the gain in kinetic energy of polymer chain, which causes increased segmental mobility of matrix.

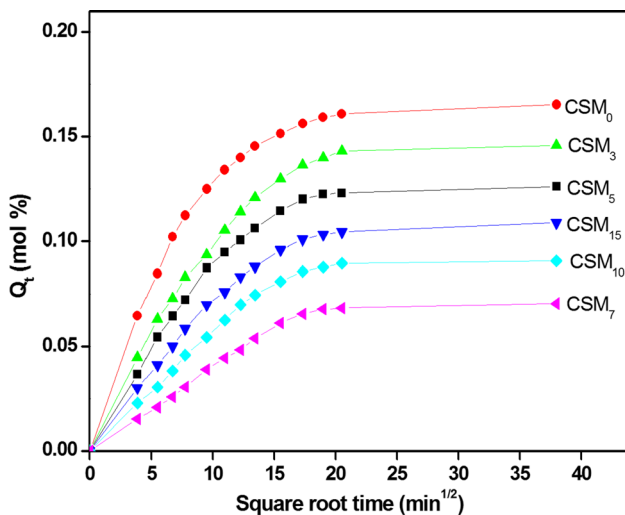


Figure 7 Sorption curves of Cl-SBR/ MnWO_4 nanocomposite through petrol at room temperature.

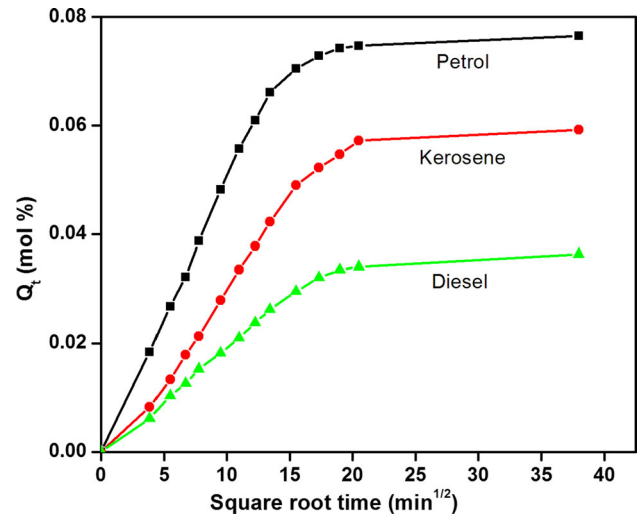


Figure 8 Solvent uptake of Cl-SBR with 7 phr of MnWO_4 in different industrial solvents.

Extent of reinforcement by theoretical modeling

The extent of reinforcement of fillers in the composites can be calculated by using Lorentz and Park equation [45]

$$\frac{Q_f}{Q_g} = ae^{-z} + b \quad (2)$$

where Q_f and Q_g denote the amount of the solvent sorbed by the nanocomposite and the pure sample, z denotes the weight of filler per unit weight of the matrix, and a and b are the constant. The Q_f/Q_g of samples is investigated using petrol as the solvent,

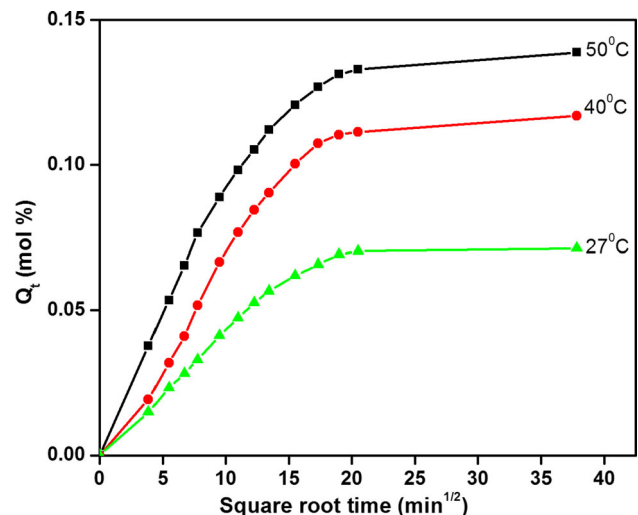


Figure 9 The mol uptake of Cl-SBR and SBR with 7 phr of MnWO_4 in petrol at different temperature.

and the ratios reflect the restriction of samples toward solvents. The ratio directly related to the extent of reinforcement and the solvent resistance of the sample. From Fig. 10, it is clear that on plotting Q_f/Q_g versus filler loading, the ratio decreases with increase in the amount of $MnWO_4$ nanoparticles. The sample with 7-phr nanoparticles shows the lowest value of Q_f/Q_g , indicating the strong matrix–filler interaction. The sample containing the lower amount of filler shows higher ratio indicates its poor matrix filler interaction.

Diffusion coefficient (D)

The kinetic parameter of the solvent sorption, the diffusion coefficient, D , is influenced by many factors such as segmental mobility of polymer matrix, nature of penetrant and amount of filler. It can be calculated using the equation [46]

$$D = \pi \left(\frac{h\theta}{Q_\infty} \right)^2 \quad (2)$$

where ‘ h ’ indicates the thickness of the sample, ‘ θ ’ is the slope of the initial linear portion of the curve which is obtained on plotting Q_t versus square root time, and ‘ Q_∞ ’ is the equilibrium absorption. From Table 3, it is seen that the D values decrease with the increase in the amount of $MnWO_4$ nanofiller. Upon the addition of nanofillers to CI-SBR matrix, the compactness of the sample increases, and the improvement in interfacial interaction between the polymer and filler restricts the local movement of

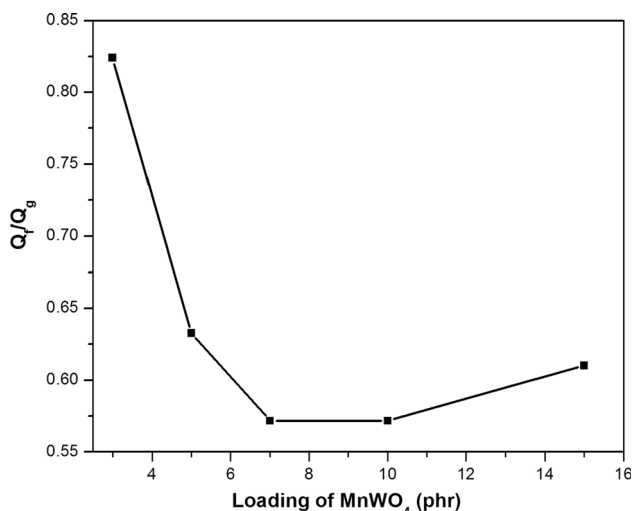


Figure 10 The extent of reinforcement of the composite using Lorentz and Park equation.

polymer chains. This reduces the equilibrium uptake, and hence, diffusion coefficient decreases with the increase in filler loading [47]. The CI-SBR/7 phr $MnWO_4$ nanocomposite has the minimum solvent uptake and hence the minimum D value due to the strong and effective interaction between CI-SBR matrix and $MnWO_4$ nanofiller. Diffusion coefficient also shows the variation in the nature of solvents, i.e., petrol has maximum and diesel has the least penetrating effect. The decrease in D values in accordance with the molar volume of solvents can be explained on the basis of free volume theory. For large molecules, higher activation energy is needed for the exchange of voids in between the macromolecular chain of CI-SBR and selected solvent [48].

Sorption coefficient (S)

The sorption coefficient S is calculated from the equation [49]

$$S = \frac{W_\infty}{W_p} \quad (3)$$

here W_∞ is the mass of the penetrant at equilibrium point and W_p is the weight of CI-SBR used for the diffusion study. The sorption coefficient also registers a decrease with the addition of $MnWO_4$ nanoparticles, and the composite containing 7 phr of filler shows the minimum value of sorption coefficient. From Table 3, it is clear that the sorption coefficient shows the same trend as that of diffusion coefficients in petroleum fuels.

Permeation coefficient (P)

The amount of solvent permeated through the unit area of polymer matrix per second is the permeation coefficient. It signifies the solvent transport through successive layers in a polymer sample. It is obtained by the multiplication of sorption coefficient and diffusion coefficient. Table 3 depicts the decrease in permeation coefficient values with increasing the $MnWO_4$ nanofiller loading. Mathematically, this is due to the decrease in D and the physical reason is the restriction to the permeation process of the solvent created by a strong interface in filled CI-SBR samples. The composite containing 7 phr of $MnWO_4$ and the gum sample (CI-SBR without filler) exhibits the minimum and maximum permeation coefficients, respectively.

Table 3 *D*, *S* and *P* values of Cl-SBR and Cl-SBR/MnWO₄ nanocomposites

Samples	Diffusion coefficient $D \times 10^5$ (cm ² /s)			Sorption coefficient <i>S</i> (mol%)			Permeation coefficient $P \times 10^5$ (cm ² /s)		
	Petrol	Kerosene	Diesel	Petrol	Kerosene	Diesel	Petrol	Kerosene	Diesel
CSM ₀	1.46	1.41	1.32	1.15	1.12	1.09	1.68	1.58	1.44
CSM ₃	1.41	1.37	1.22	1.12	1.07	1.06	1.58	1.47	1.29
CSM ₅	1.35	1.32	1.18	1.08	1.03	1.01	1.46	1.35	1.19
CSM ₇	1.21	1.19	1.08	1.01	0.91	0.86	1.22	1.08	0.93
CSM ₁₀	1.25	1.23	1.14	1.05	0.96	0.89	1.31	1.18	1.01
CSM ₁₅	1.27	1.25	1.16	1.06	0.99	0.92	1.34	1.23	1.06

Activation energy of diffusion (E_D) and permeation (E_P)

The activation energy of diffusion and permeation can be calculated from the Arrhenius equation

$$X = X_0 e^{-E_x/RT} \quad (4)$$

The values of *D* or *P* obtained at 27, 40 and 50 °C are substituted instead of *X* to get enthalpy of diffusion or permeation, respectively. In order to take place diffusion or permeation of solvents, there should be free volume inside the matrix, or a diffusional jump occurs in the presence of free voids inside the matrix [50]. It requires high activation energy and is obtained from the slopes of the curve plotted as log *D* versus 1/*T*. From Table 4, the E_P and E_D values are found increasing in accordance with the filler loading and penetrant size. Due to the large molecular size diesel requires more activation energy to penetrate. The free volume of the polymer decreases with increasing the filler content due to high compactness which results in higher activation energy. From the table, it is clear that the Cl-SBR without filler has the minimum activation energy of diffusion and permeation, and the composite with 7 phr of MnWO₄ shows highest activation energy. There is a decrease in activation energy upon further addition of nanoparticles beyond 7 phr.

Thermodynamic parameters

Enthalpy (ΔH_s) and entropy (ΔS_s) of sorption of petroleum fuels in MnWO₄-filled Cl-SBR composites have been studied using the equilibrium sorption constant (K_s), which is obtained by dividing the number of moles of solvent sorbed at equilibrium with the weight of the polymer sample. Thus,

Table 4 E_D and E_P values of Cl-SBR and Cl-SBR/MnWO₄ nanocomposites

Samples	Petrol		Kerosene		Diesel	
	E_D	E_P	E_D	E_P	E_D	E_P
CSM ₀	6.52	5.29	6.64	5.38	6.82	5.52
CSM ₃	6.58	5.34	6.69	5.43	6.94	5.58
CSM ₅	6.73	5.41	6.77	5.49	6.99	5.63
CSM ₇	6.92	5.59	7.08	5.69	7.23	5.77
CSM ₁₀	6.81	5.47	6.89	5.56	7.12	5.71
CSM ₁₅	6.77	5.45	6.81	5.51	7.08	5.67

substituting the values of K_s in Van't Hoff's equation the enthalpy and entropy of sorption can be calculated as [51]

$$\log K_s = \frac{\Delta S_s}{2.303R} - \frac{\Delta H_s}{2.303RT} \quad (5)$$

Plots of log K_s against 1/*T* give a straight line where the slopes and intercept yield ΔH_s and ΔS_s , respectively. These values are shown in Table 5. All the composites in three solvents show an endothermic enthalpy change (positive ΔH_s). The enthalpy change increases from petrol to diesel, and the results obtained are in good agreement with the values obtained from E_P and E_D ($\Delta H = E_P - E_D$). The entropy change of diffusion is also found positive, and on increasing filler loading the entropy change decreases. The composite filled with 7 phr of MnWO₄ has strong interfacial interaction between polymer and filler; hence, it shows minimum entropy. By using the values of ΔH_s and ΔS_s the Gibbs free energy can be calculated ($\Delta G_s = \Delta H_s - T\Delta S_s$). It is found that the free energy of diffusion enhanced by increasing the amount of MnWO₄; hence, the Cl-SBR

without filler and with 7 phr of filler shows the minimum and maximum free energy of sorption. The values obtained reveal the fact that the spontaneity in the diffusion solvent decreases upon reinforcement with nanoparticles [52].

Transport mechanism

The mechanism of transport can be calculated from the equation [53]

$$\log \frac{Q_t}{Q_\infty} = \log k + n \log t \tag{6}$$

where Q_t and Q_∞ are the mol uptake of solvents at time t and at the equilibrium. The polymer–solvent relationship can be investigated by using the constant k which depends on the structural characteristics of the polymeric material and is given in Table 6. The value of n indicates the mode of transport, and when the value of n is 0.5, mode of transport is said to be Fickian; if it is in between 0.5 and 1, then it is in anomalous mode. It may be due to the coupling of Fickian and non-Fickian mode of transport [54]. Here reinforcement of Cl-SBR matrix with nanoparticles makes the chain relaxation very slow due to the high viscosity of the system. Hence, the mode of transport becomes anomalous as indicated by ‘ n ’ values in Table 6. It is very clear from Table 6 that the structural parameter k is decreased with increase in $MnWO_4$ nanofiller loading which is a clear evidence for reinforcement and this result is in accordance with our previous study [55]. From the k values obtained, we can see that in the presence of nanoparticles the solvent matrix interaction becomes very weak as compared to the pure Cl-SBR matrix. The lowest value of k is shown by the composite with 7 phr of $MnWO_4$ nanoparticles which can be a strong support for uniform distribution of nanoparticles. This is supported by SEM micrographs also. It also

ensures the compactness of the samples upon reinforcement. Owing to the same reason, the values of k decrease with increasing the molar mass of the solvents [56]. In the present study, petrol shows the maximum and diesel shows the minimum value of k .

Conclusions

Chlorinated styrene butadiene rubber with different contents of $MnWO_4$ nanocomposites was prepared by a simple two-roll mill mixing. The curing behavior, mechanical, thermal, electrical, oil resistance, solvent sorption and transport properties of Cl-SBR/ $MnWO_4$ nanocomposite vulcanizates were analyzed with respect to the different loading of nanofillers. The addition of nanofiller to Cl-SBR reduces the amorphous nature of Cl-SBR. The increased compactness of or reduced flexibility of the samples increased the glass transition temperature of Cl-SBR from -35 to -29 °C. The reduction in optimum cure time of Cl-SBR noted with the increasing loading of nanoparticles proved to be beneficial to enhance the production rate of articles using these compositions. The improved tensile strength, modulus and tear strength values with the loading of nanoparticles up to 7 phr were attributed to the formation of a strong interface with the large interfacial area. The uniform distribution of nanoparticles in Cl-SBR matrix (7-phr loading) was evident from SEM analysis. In addition, the electrical conductivity was also found to be highest at this loading, thus opening the possibility to use these materials as future semiconducting materials with easy processability. The studies based on the absorption of ASTM oils as well as petroleum fuels support the excellent reinforcement of Cl-SBR matrix at 7-phr loading of $MnWO_4$ particles, meanwhile reflecting the reduced absorption of solvent with higher molecular weight and size. Overall, an

Table 5 ΔH , ΔS and ΔG of Cl-SBR and Cl-SBR/ $MnWO_4$ nanocomposites

Samples	ΔH			ΔS			ΔG		
	Petrol	Kerosene	Diesel	Petrol	Kerosene	Diesel	Petrol	Kerosene	Diesel
CSM ₀	1.24	1.29	1.36	0.051	0.046	0.037	14.06	12.51	9.74
CSM ₃	1.27	1.36	1.47	0.048	0.037	0.031	13.13	9.74	7.83
CSM ₅	1.32	1.43	1.52	0.042	0.032	0.025	11.28	8.17	5.98
CSM ₇	1.54	1.69	1.73	0.021	0.018	0.012	4.76	3.44	1.87
CSM ₁₀	1.44	1.56	1.66	0.032	0.024	0.019	8.16	5.64	4.04
CSM ₁₅	1.39	1.51	1.62	0.039	0.029	0.021	10.31	7.19	4.68

Table 6 n and k values of Cl-SBR and Cl-SBR/MnWO₄ nanocomposites

Samples	Petrol		Kerosene		Diesel	
	n	$k \times 10^2$ (min ⁻¹)	n	$k \times 10^2$ (min ⁻¹)	n	$k \times 10^2$ (min ⁻¹)
CSM ₀	0.75	0.22	0.76	0.21	0.82	0.19
CSM ₃	0.77	0.21	0.83	0.19	0.86	0.18
CSM ₅	0.78	0.18	0.81	0.17	0.89	0.16
CSM ₇	0.78	0.16	0.87	0.14	0.94	0.12
CSM ₁₀	0.73	0.17	0.86	0.16	0.93	0.14
CSM ₁₅	0.75	0.18	0.79	0.17	0.92	0.15

anomalous diffusion mechanism was revealed from the study of solvent transport in Cl-SBR and its nanocomposites. The Lorentz and Park model supports the high reinforcing ability of MnWO₄ nanoparticles in Cl-SBR, and the extent of reinforcement was higher in 7-phr composite.

Acknowledgements

The authors wish to thank Prof. P. P. Pradyumnan, Department of Physics, University of Calicut, and Prof. P. Pradeep, Department of Physics, NIT Calicut, for providing necessary facilities in the department.

References

- Li Y, Wang Q, Wang T, Pan G (2012) Preparation and tribological properties of graphene oxide/nitrile rubber nanocomposites. *J Mater Sci* 47:730–738. <https://doi.org/10.1007/s10853-011-5846-4>
- Cho CH, Cho MS, Sung JH, Choi HJ, Jhon MS (2004) Preparation and characterization of poly (vinyl butyral)/Na⁺-montmorillonite nanocomposite. *J Mater Sci* 39:3151–3153. <https://doi.org/10.1023/B:JMSC.0000025846.88346.0a>
- Tang Z, Zhang C, Zhu L, Guo B (2016) Low permeability styrene butadiene rubber/boehmite nanocomposites modified with tannic acid. *Mater Des* 103:25–31
- Kar S, Maji PK, Bhowmick AK (2010) Chlorinated polyethylene nanocomposites: thermal and mechanical behavior. *J Mater Sci* 45:64–71. <https://doi.org/10.1007/s10853-009-3891-z>
- Gómez M, Bracho D Palza H, Quijada R (2015) Effect of morphology on the permeability, mechanical and thermal properties of polypropylene/SiO₂ nanocomposites. *Polym Int* 64:1245–1251
- Ye HJ, Shao WZ, Zhen L (2013) Crystallization kinetics and phase transformation of poly (vinylidene fluoride) films incorporated with functionalized BaTiO₃ nanoparticles. *J Appl Polym Sci* 129:2940–2949
- Ramesan MT, Jose C, Jayakrishnan P, Anilkumar T (2018) Multifunctional ternary composites of poly (vinyl alcohol)/cashew tree gum/pumice particles. *Polym Compos* 39:38–45
- Fu SY, Feng XQ, Lauke B, Mai YW (2008) Effects of particle size, particle/matrix interface adhesion and particle loading on mechanical properties of particulate–polymer composites. *Compos B* 39:933–961
- Goren K, Chen L, Schadler LS, Ozisik R (2010) Influence of nanoparticle surface chemistry and size on supercritical carbon dioxide processed nanocomposite foam morphology. *J Supercrit Fluids* 51:420–427
- Wan C, Chen B (2012) Reinforcement and interphase of polymer/graphene oxide nanocomposites. *J Mater Chem* 22:3637–3646
- Brosseau C, Molinie P, Boulic F, Carmona F (2001) Mesostructure, electron paramagnetic resonance and magnetic properties of polymer carbon black composites. *J Appl Phys* 89:8297–8310
- Boulic F, Brosseau C, Mest YL, Loaec J, Carmona F (1998) Absorbency properties and electron paramagnetic resonance characterization of polymeric carbon black composites. *J Phys D Appl Phys* 31:1904–1912
- Brosseau C, Boulic F, Queffelec P, Bourbigot C, Mest YL, Loaec J, Beroual A (1997) Dielectric and microstructure properties of polymer carbon black composites. *J Appl Phys* 81:882–891
- Lee KM, Weissgarber T, Kieback B (2004) Microstructural and chemical properties of AlN–Cu nanocomposite powders prepared by planetary ball milling. *J Mater Sci* 39:5235–5238. <https://doi.org/10.1023/B:JMSC.0000039217.45509.11>
- Schubert U (2009) Preparation of metal oxide or metal nanoparticles in silica via metal coordination to organofunctional trialkoxysilanes. *Polym Int* 58:317–322
- Changjie Y, Zhang Q, Junwei G, Junping Z, Youqiang S, Yuhang W (2011) Cure characteristics and mechanical properties of styrene-butadiene rubber/hydrogenated

- acrylonitrile-butadiene rubber/silica composites. *J Polym Res* 18:2487–2494
- [17] Das A, Costa FR, Wagenknecht U, Heinrich G (2008) Nanocomposites based on chloroprene rubber: effect of chemical nature and organic modification of nanoclay on the vulcanizate properties. *Eur Polym J* 44:3456–3465
- [18] Viet CX, Ismail H, Rashid AA, Takeichi T, Thao VH (2008) Organoclay filled natural rubber nanocomposites: the effects of filler loading. *Polym Plast Technol Eng* 47:1090–1096
- [19] Ramesan MT (2014) Flammability, oil resistance, and interaction of petroleum fuels with dichlorocarbene modified styrene butadiene rubber/fly ash composites. *Pet Sci Technol* 32:1775–1783
- [20] Li H, Sun J, Song Y, Zheng Q (2009) The mechanical and viscoelastic properties of SBR vulcanizates filled with organically modified montmorillonite and silica. *J Mater Sci* 44:1881–1888. <https://doi.org/10.1007/s10853-008-3223-8>
- [21] Guo L, Huang G, Zheng J, Li G (2014) Effect of nanosilica on thermal oxidative degradation of SBR. *J Therm Anal Calorim* 116:359–366
- [22] Ramesan MT, Alex R (2000) Dichlorocarbene modified SBR—vulcanization behaviour and physical properties. *Kautsch Gummi Kunstst* 53:596–600
- [23] Ramesan MT, Alex R (1998) Dichlorocarbene modification of styrene-butadiene rubber. *J Appl Polym Sci* 68:153–160
- [24] Ahmadi M, Shojaei A (2015) Reinforcing mechanisms of carbon nanotubes and high structure carbon black in natural rubber/styrene-butadiene rubber blend prepared by mechanical mixing—effect of bound rubber. *Polym Int* 64:1627–1638
- [25] Cho BM, Kim GH (2010) Effect of the processing parameters on the surface resistivity of acrylonitrile-butadiene rubber/multiwalled carbon nanotube. *J Appl Polym Sci* 116:555–561
- [26] Jasna VC, Ramesan MT (2017) Studies on the mechanical, electrical properties and interaction of petroleum fuels with SBR/manganous tungstate nanocomposites. *J Inorg Organomet Polym* 27:968–978
- [27] Khaksar M, Boghaei DM, Amini M (2015) Synthesis, structural characterization and reactivity of manganese tungstate nanoparticles in the oxidative degradation of methylene blue. *C R Chim* 18:199–203
- [28] Paul PK, Hussain SA, Bhattacharjee D, Pal M (2013) Preparation of polystyrene-clay nanocomposite by solution intercalation technique. *Bull Mater Sci* 36:361–366
- [29] Ramesan MT, Santhi V (2018) Synthesis, characterization, conductivity, thermal properties and sensor application study of polypyrrole/silver doped nickel oxide nanocomposites. *Comp Interfaces*. <https://doi.org/10.1080/09276440.2018.1439626>
- [30] Bussu G, Lazzeri A (2006) On the use of dynamic mechanical thermal analysis (DMTA) for measuring glass transition temperature of polymer matrix fibre reinforced composites. *J Mater Sci* 41:6072–6076. <https://doi.org/10.1007/s10853-006-0694-3>
- [31] Lakshminarayanan S, Gelves GA, Sundraraj U (2012) Vulcanization behavior and mechanical properties of organoclay fluoroelastomer nanocomposites. *J Appl Polym Sci* 124:5056–5063
- [32] Ji XL, Jing JK, Jiang W, Jiang BZ (2002) Tensile modulus of polymer nanocomposites. *Polym Eng Sci* 42:983–993
- [33] Wang M, Fan X, Thitsartam W, He C (2015) Rheological and mechanical properties of epoxy/clay nanocomposites with enhanced tensile and fracture toughness. *Polymer* 58:43–52
- [34] Ramesan MT, Jayakrishnan P, Anilkumar T, Mathew G (2018) Influence of copper sulphide nanoparticles on the structural, mechanical and dielectric properties of poly (vinyl alcohol)/poly (vinyl pyrrolidone) blend nanocomposites. *J Mater Sci Mater Electron* 29:1992–2000
- [35] Eckersley ST, Chaput B (2001) Tensile properties of elastomeric polyolefin thin films: the path to failure. *J Appl Polym Sci* 80:2545–2557
- [36] Jong L (2016) Particle size and particle-particle interactions on tensile properties and reinforcement of corn flour particles in natural rubber. *Eur Polym J* 74:136–147
- [37] Gorrasi G, Piperopoulos E, Lanza M, Milone C (2013) Effect of morphology of the filler on the electrical behaviour of poly (L-lactide) nanocomposites. *J Phys Chem Solids* 74:1–6
- [38] Ramesan MT, Santhi V (2017) In situ synthesis, characterization, conductivity studies of polypyrrole/silver doped zinc oxide nanocomposites and their application for ammonia gas sensing. *J Mater Sci Mater Electron* 28:18804–18814
- [39] Abraham J, Muraleedharan K, Kumar CR, Thomas S, George SC (2017) Solvent transport characteristics of thermoplastic elastomer blends based on nylon and NBR. *Polym Eng Sci* 57:231–236
- [40] George SC, Knorgen M, Thomas S (1999) Effect of nature and extent of crosslinking on swelling and mechanical behavior of styrene-butadiene rubber membranes. *J Membr Sci* 163:1–17
- [41] Moly KA, Bhagawan SS, George SC, Thomas S (2007) Sorption and diffusion of aromatic solvents through linear low density polyethylene-ethylene vinyl acetate blend membranes. *J Mater Sci* 42:4552–4561. <https://doi.org/10.1007/s10853-006-0544-3>
- [42] Hwang KK, Ryu SH, Hong SU (2002) Diffusion and sorption behavior of glycidyl methacrylate in styrene butadiene rubber. *J Appl Polym Sci* 86:2701–2706

- [43] John J, Kunchandy S, Kumar K, Pius A, Thomas S (2010) Transport of methyl methacrylate monomer through natural rubber. *J Mater Sci* 45:409–419. <https://doi.org/10.1007/s10853-009-3956-z>
- [44] Tung WS, Griffin PJ, Meth JS, Clarke N, Composto RJ, Winey KI (2016) Temperature-dependent suppression of polymer diffusion in polymer nanocomposites. *ACS Macro Lett* 5:735–739
- [45] James J, Thomas GV, Pramoda KP, Thomas S (2017) Transport behaviour of aromatic solvents through styrene butadiene rubber/poly [methyl methacrylate] (SBR/PMMMA) interpenetrating polymer network (IPN) membranes. *Polymer* 116:76–88
- [46] Ramesan MT (2014) Effect of fly ash on thermal stability, flammability, oil resistance and transport properties of chlorinated styrene butadiene rubber composites. *J Elastom Plast* 46:303–324
- [47] Geethamma VG, Thomas S (2005) Diffusion of water and artificial seawater through coir fiber reinforced natural rubber composites. *Polym Compos* 26:136–143
- [48] Padhi S, Achary PGR, Nayak NC (2015) Molecular transport behaviour of organic solvents through halloysite nanotubes filled ethylene-vinyl acetate copolymer. *Bull Mater Sci* 38:925–933
- [49] Stephen R, Joseph K, Oommen Z, Thomas S (2007) Molecular transport of aromatic solvents through microcomposites of natural rubber (NR), carboxylated styrene butadiene rubber (XSBR) and their blends. *Compos Sci Technol* 67:1187–1194
- [50] Sareena C, Sreejith MP, Ramesan MT, Purushothaman E (2015) Transport properties of coconut shell powder (CSP) reinforced natural rubber composites in aromatic solvents. *Polym Bull* 72:1683–1702
- [51] Sujith A, Unnikrishnan G (2005) Barrier properties of natural rubber/ethylene vinyl acetate/carbon black composites. *J Mater Sci* 40:4625–4640. <https://doi.org/10.1007/s10853-005-0904-4>
- [52] Sareena C, Ramesan MT, Purushothaman E (2013) Transport studies of peanut shell powder reinforced natural rubber composites in chlorinated solvents. *Fibers Polym* 14:1674–1687
- [53] Hedenqvist MS, Backman A, Gällstedt M, Boyd RH, Gedde UW (2006) Morphology and diffusion properties of whey/montmorillonite nanocomposites. *Compos Sci Technol* 66:2350–2359
- [54] Alva LR, Montiel AG, Vega MJA (2016) Diffusion of organic volatile molecules in LDPE/halloysite nanocomposites. *Polym Compos* 37:1267–1273
- [55] Jasna VC, Ramesan MT (2018) Fabrication of novel nanocomposites from styrene butadiene rubber/zinc sulphide nanoparticles. *J Mater Sci* 53:8250–8262. <https://doi.org/10.1007/s10853-018-2173-z>
- [56] Kumar PVA, Kumar SA, Varughese KT, Thomas S (2012) Transport properties of high-density polyethylene/ethylene propylene diene terpolymer blends. *J Mater Sci* 47:3293–3304. <https://doi.org/10.1007/s10853-011-6168-2>